ADP-ribosylation factor–like 4C binding to filamin-A modulates filopodium formation and cell migration

Tsai-Shin Chiang[a], Hsu-Feng Wu[a], and Fang-Jen S. Lee[a,b,*]
[a]Institute of Molecular Medicine, College of Medicine, National Taiwan University, 100 Taipei, Taiwan; [b]Department of Medical Research, National Taiwan University Hospital, 100 Taipei, Taiwan

ABSTRACT **Changes in cell morphology and the physical forces that occur during migration are generated by a dynamic filamentous actin cytoskeleton. The ADP-ribosylation factor–like 4C (Arl4C) small GTPase acts as a molecular switch to regulate morphological changes and cell migration, although the mechanism by which this occurs remains unclear. Here we report that Arl4C functions with the actin regulator filamin-A (FLNa) to modulate filopodium formation and cell migration. We found that Arl4C interacted with FLNa in a GTP-dependent manner and that FLNa IgG repeat 22 is both required and sufficient for this interaction. We also show that interaction between FLNa and Arl4C is essential for Arl4C-induced filopodium formation and increases the association of FLNa with Cdc42-GEF FGD6, promoting cell division cycle 42 (Cdc42) GTPase activation. Thus our study revealed a novel mechanism, whereby filopodium formation and cell migration are regulated through the Arl4C-FLNa–mediated activation of Cdc42.**

Monitoring Editor
Laurent Blanchoin
CEA Grenoble

Received: Jan 23, 2017
Revised: Aug 17, 2017
Accepted: Aug 25, 2017

INTRODUCTION

ADP-ribosylation factors (Arfs), small GTP-binding proteins of the Ras superfamily, regulate vesicular transport, membrane trafficking, organelle structure, and cytoskeletal remodeling through activation via guanine nucleotide-exchange factors (GEFs) and inactivation via GTPase-activating proteins (GAPs) (Moss and Vaughan, 1998; Donaldson and Jackson, 2000; Jackson and Casanova, 2000; Takai *et al.*, 2001; Burd *et al.*, 2004; D'Souza-Schorey and Chavrier, 2006). Arf-like proteins (Arls) exhibit 50–60% amino acid identity with Arfs (Kahn *et al.*, 2006), and 20 proteins belonging to this subfamily have been identified to date. Owing to their unique structures, including a nuclear localization signal at the C-terminus and a long interswitch region between two switch domains, Arl4s are distinct from other Arfs/Arls (Pasqualato *et al.*, 2002). Constituting the subfamily, Arl4A, Arl4C, and Arl4D have different expression patterns depending on the developmental process (Schurmann *et al.*, 1994; Jacobs *et al.*, 1999; Lin *et al.*, 2000, 2002). Our previous studies showed that Arl4A and Arl4D modulate actin cytoskeleton remodeling and cell migration (Li *et al.*, 2007; Patel *et al.*, 2011). Recently Matsumoto *et al.* (2014) reported that expression of Arl4C in normal epithelial cells promotes migration and proliferation, and these authors suggested that Arl4C is involved in epithelial morphogenesis. However, the mechanisms by which Arl4C affects cell morphology and motility remain unclear.

Crucial to many cellular processes, such as embryonic morphogenesis, tissue repair, wound healing, organ development, and tumor metastasis, cell migration is a highly regulated event that is initiated by protrusion of the cell membrane (Lauffenburger and Horwitz, 1996; Friedl and Wolf, 2003). The Rho GTPase family is considered to play the major role in regulating cell migration and actin reorganization (Heasman and Ridley, 2008), and the well-studied family member Cdc42 is involved in filopodium formation, which is closely related to cell motility (Fernandez *et al.*, 2013; Melendez *et al.*, 2013). The changes in cell morphology and physical forces that occur during migration or cell division are generated in part by a dynamic cytoskeleton composed of filamentous actin (F-actin). Indeed, the actin cytoskeleton is intimately involved in both the formation and maintenance of cell shape and morphology in response to various signals or stimuli. One actin-binding protein, filamin (FLN) (Lauffenburger and Horwitz, 1996), a well-known scaffold protein

This article was published online ahead of print in MBoC in Press (http://www.molbiolcell.org/cgi/doi/10.1091/mbc.E17-01-0059) on August 30, 2017.
The authors declare no competing financial interests.
*Address correspondence to: Fang-Jen S. Lee (fangjen@ntu.e du.tw)
Abbreviations used: Arf, ADP-ribosylation factor; Arl, ADP-ribosylation factor-like.

that functions in F-actin cross-linking, receptor anchoring, and cell signaling (Zhou *et al.*, 2010; Nakamura *et al.*, 2011), can mediate dynamic actin remodeling. The FLN family consists of three homologous proteins, FLNa, FLNb, and FLNc (Zhou *et al.*, 2010; Nakamura *et al.*, 2011), with FLNa being the most abundant and widely distributed in humans. FLNa is composed of an N-terminal actin-binding domain (ABD) followed by 24 immunoglobulin (Ig)-like tandem repeats; dimerization is mediated by IgG repeat 24 located near the C-terminus (van der Flier and Sonnenberg, 2001; Himmel *et al.*, 2003; Seo *et al.*, 2009). More than 70 cellular proteins, including channels, receptors, signaling molecules, and transcription factors, have been identified as FLNa-interacting partners (Stossel *et al.*, 2001; Zhou *et al.*, 2010; Nakamura *et al.*, 2011). Although most interact with the C-terminus of FLNa, F-actin mainly interacts with the N-terminal ABD of FLNa to assist in the cross-linking of F-actin into networks of orthogonally branched filaments (Zhou *et al.*, 2010; Nakamura *et al.*, 2011). By cross-linking cytoskeletal actin into three-dimensional networks, FLNa functions as a signaling scaffold and a mechano-sensor of extrinsic shear forces. Many researchers have also reported that FLNa functions as an adaptor protein that links the cell membrane to the cytoskeleton via interactions with transmembrane proteins and cell-surface receptors (Gehler *et al.*, 2009; Lynch *et al.*, 2011; Nakamura *et al.*, 2011).

In this study, we identified FLNa as a novel effector of Arl4C and found FLNa to be required for Arl4C-induced filopodium formation and cell migration. We show here that FLNa-knockdown results in decreased filopodium formation and cell migration, which can be rescued by expression of wild-type FLNa but not by an FLNa mutant deficient in Arl4C binding. Furthermore, the Arl4C-FLNa interaction promotes Cdc42 activation by increasing the association of Cdc42-GEF FGD6 with FLNa. Our results demonstrate that Arl4C functions with FLNa to modulate the formation of filopodia and cell migration by promoting activation of Cdc42.

RESULTS

Arl4C interacts with filamin-A in a GTP-dependent manner

To identify potential effectors of Arl4C, Arl4C-Q72L, a GTP-bound form of Arl4C, was used as bait to screen a human fetal brain cDNA library in a yeast two-hybrid system. Several candidates were identified, two of which contain a C-terminal fragment (residues 2363–2646) spanning IgG repeat 22 (R22) to IgG repeat 24 (R24) of FLNa. To determine the specific regions of FLNa responsible for its interaction with Arl4C, fragments for different regions of FLNa R22-R24 were generated and their interaction with Arl4C was tested in a yeast two-hybrid assay (Figure 1A). Only the FLNa-R22′ region, but not R23 or R24, was found to interact with Arl4C-Q72L (Figure 1B), indicating that the FLNa-R22′ region is sufficient for interaction with Arl4C. In addition, FLNa-R22′ was able to interact with Arl4C-WT and Arl4C-Q72L, but not with the Arl4C-T44N mutant defective in GTP binding (Figure 1C), suggesting that Arl4C interacts with FLNa R22′ in a GTP-dependent manner.

An in vitro pull-down assay was then used to confirm the interaction between Arl4C and FLNa. As shown in Figure 1D, Arl4C-WT and Arl4C-Q72L, but not Arl4C-T44N, were pulled down by GST-FLNa-R22′. The interaction was also verified by an in vivo coimmunoprecipitation assay in which HeLa cells transiently transfected with Arl4C and its mutants were immunoprecipitated using magnetic beads conjugated with an anti-FLNa antibody. Again, Arl4C-WT and Arl4C-Q72L, but not Arl4C-T44N, were coimmunoprecipitated with endogenous FLNa (Figure 1E). In contrast, little or no interaction with the FLNa-R22′ region was observed with the other two Arl4 family members, Arl4A and Arl4D, by either yeast two-hybrid (Figure 1F) or pull-down (Figure 1G) assays. These results demonstrate that Arl4C specifically interacts with FLNa in a GTP-dependent manner.

The IgG repeat 22 of FLNa is required for Arl4C-FLNa interaction

To identify residues in the FLNa-R22′ region that are critical for its interaction with Arl4C, 13 mutants of FLNa R22′ (A1–A13), in which five to six amino acids were sequentially substituted by alanine (Figure 2A), were assessed in yeast two-hybrid assays. Only FLNa R22′-A1, -A3, -A5, -A7, and -A13 were able to interact with Arl4C-Q72L (Figure 2B). FLNa-R22′-A2 and FLNa R22′-A10 were then selected for further analysis to determine the importance of certain residues of FLNa in the Arl4C-WT interaction. As presented in Figure 2C, Arl4C was pulled down in vitro by GST-FLNa R22′-WT and GST-FLNa R22′-A2, but was much less so by GST-fused FLNa R22′-A10. Notably, the GST-FLNa R22′-A2 beads pulled down less Arl4C protein than the FLNa R22′-WT beads, suggesting that FLNa R22′-A10 plays a more critical role in the Arl4C-FLNa interaction than FLNa R22′-A2.

Arl4C-FLNa interaction is necessary for filopodium formation

As it has been reported that depletion of Arl4C reduces cancer cell migration (Fujii *et al.*, 2014; Su *et al.*, 2015), different forms of Arl4C were expressed in HeLa cells to investigate the possible effects of Arl4C on the membrane structure. Figure 3A shows that expression of Arl4C-WT or Arl4C-Q72L induced membrane protrusion structures and filopodium formation, and notably, both Arl4C-WT and Arl4C-Q72L were concentrated at the site of membrane protrusion and colocalized with FLNa. Conversely, Arl4C-T44N was found mainly in the cytosol. In addition, both Arl4C-WT- and Arl4C-Q72L-induced filopodium are highly colocalized with the F-actin probe phalloidin and fascin (Figure 3, B and C). These results indicate that Arl4C induces membrane protrusion and filopodium formation and localizes at the plasma membrane in a GTP-dependent manner.

To investigate whether FLNa is involved in Arl4C-induced filopodium formation and cell migration, Arl4C was first transfected into FLNa+ cell lines (isogenic FLNa+ cell line A7) and the FLNa-M2 cell line (FLNa-deficient cells) (Cunningham *et al.*, 1992). Compared to untransfected cells, overexpression of Arl4C induced the formation of filopodia in the A7 cells (Figure 4A) but not in the M2 cells (Figure 4B). These results indicate that FLNa is critical for Arl4C-induced filopodium formation. To investigate whether interaction between Arl4C and FLNa is important for the formation of filopodia, we examined M2 cells cotransfected with Arl4C and FLNa-WT, FLNa-A2, or FLNa-A10, respectively. Filopodium formation was rescued by coexpressing Arl4C and FLNa-WT in M2 cells (Figure 4B). However, only a few filopodium structures were observed in M2 cells coexpressing Arl4C and FLNa-A2. In contrast, much less filopodium formation occurred in cells coexpressing Arl4C and FLNa-A10. The number of filopodia was significantly reduced in FLNa-A2 and -A10 when compared with FLNa-WT. These results indicate that the Arl4C-FLNa interaction is necessary for filopodium formation.

Arl4C-FLNa interaction is critical for cell migration

The GTP-dependent effect of Arl4C on cell migration was evaluated in a wound-healing assay using HeLa cells overexpressing different forms of Arl4C. The cells expressing Arl4C-WT and Arl4C-Q72L showed higher wound-healing ability, whereas those expressing Arl4C-T44N displayed a migration capacity lower than the vector control group (Figure 5, A and B). Arl4C depletion also resulted in

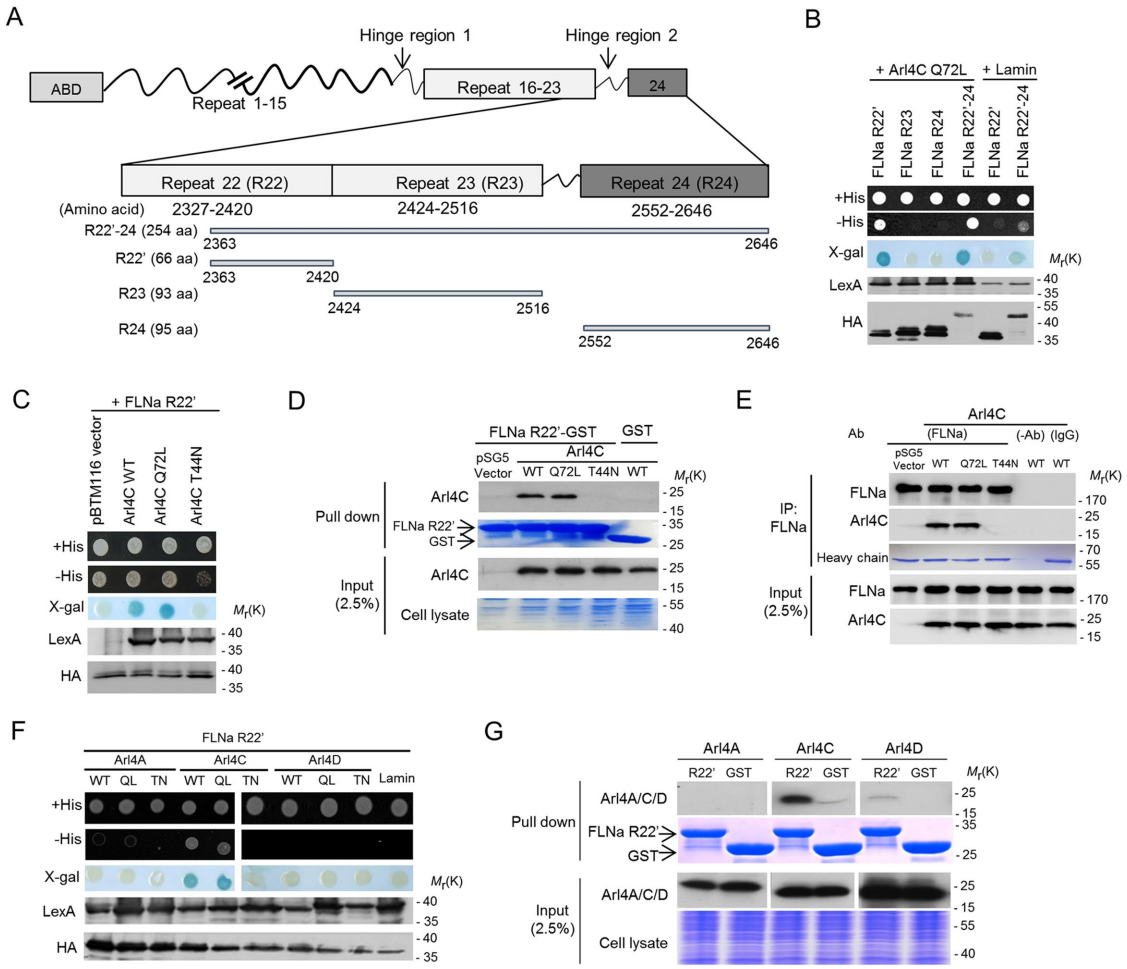

FIGURE 1: Arl4C interacts with FLNa. (A) Schematic diagram of FLNa and fragments constructed in this study. FLNa contains 24 IgG repeats and possesses an actin-binding domain (ABD) at the N-terminus. FLNa was identified according to fragments of various lengths using Arl4C-Q72L as bait in a yeast two-hybrid system. (B) Different FLNa fragments were tested for interaction with Arl4C-Q72L in yeast two-hybrid assays. The levels of proteins expressed by the transforming plasmids were confirmed by immunoblotting. Lamin was used as a negative control. After cotransformation with the indicated plasmids, interactions were verified by growth of the yeast on a synthetic His+ plate and a His– selective plate, followed by filter assays for β-galactosidase activity. Total protein (20 μg) was loaded onto a 10-well gel to detect proteins. (C) Different forms of Arl4C were tested for interaction with the FLNa R22′ region in yeast two-hybrid assays. The levels of protein expressed by the transforming plasmids were confirmed by immunoblotting. Empty vector pBTM116 was used as a negative control. (D) Interaction between WT and the GTP-bound form of Arl4C with FLNa was tested by a pull-down assay. Purified GST or FLNa R22′-GST was incubated with lysates of HeLa cells expressing Arl4C-WT, Arl4C-Q72L, and Arl4C-T44N. After binding and washing, bead-bound GST-protein complexes were analyzed by immunoblotting using an anti-Arl4C antibody. SDS–PAGE analysis of the total cell lysate and Arl4C (input) expression by immunoblotting were used to verify the initial expression level. Equal amounts of GST beads were used in each experiment as shown by Coomassie Blue staining. (E) Interaction between Arl4C and FLNa was verified by coimmunoprecipitation. HeLa cells, which possess endogenous FLNa, transiently transfected with the empty vector pSG5 or Arl4C-WT, Arl4C-Q72L, or Arl4C-T44N in pSG5 were lysed and immunoprecipitated with anti-FLNa antibody or irrelevant mouse IgG-conjugated protein G magnetic beads. The bound proteins were separated by SDS–PAGE and subjected to immunoblotting with antibodies against FLNa and Arl4C. To confirm the initial expression level, 2.5% of the total cell lysate (input) was loaded. Equal amounts of FLNa antibody were used in the assays as shown by Coomassie Blue staining of the heavy chain. (F) Wild-type and various mutants of Arl4A, Arl4C, and Arl4D were tested for interaction with FLNa R22′ in yeast two-hybrid assays. Total protein (20 μg) was loaded onto a 10-well gel to detect proteins. (G) The interaction of FLNa R22′ with the Arl4 family was tested by pull-down assays in HeLa cells. SDS–PAGE analysis of total cell lysates and expression of Arl4A/C/D (input) by immunoblotting was used to verify the initial expression level. Equal amounts of GST beads were used in each experiment as shown by Coomassie Blue staining.

decreased HeLa cells migration (Figure 5, C and D). We further examined the effect of Arl4C on cell migration in human lung epithelial carcinoma A549 cells, which express high levels of Arl4C. Depletion of Arl4C also resulted in decreased A549 cell migration, which was rescued by expression of small interfering RNA (siRNA)-resistant Arl4C (Figure 5, E and F). We then examined whether cell migration induced by Arl4C also requires FLNa by performing wound-healing and transwell migration assays. Arl4C overexpression in HeLa cells, but not in

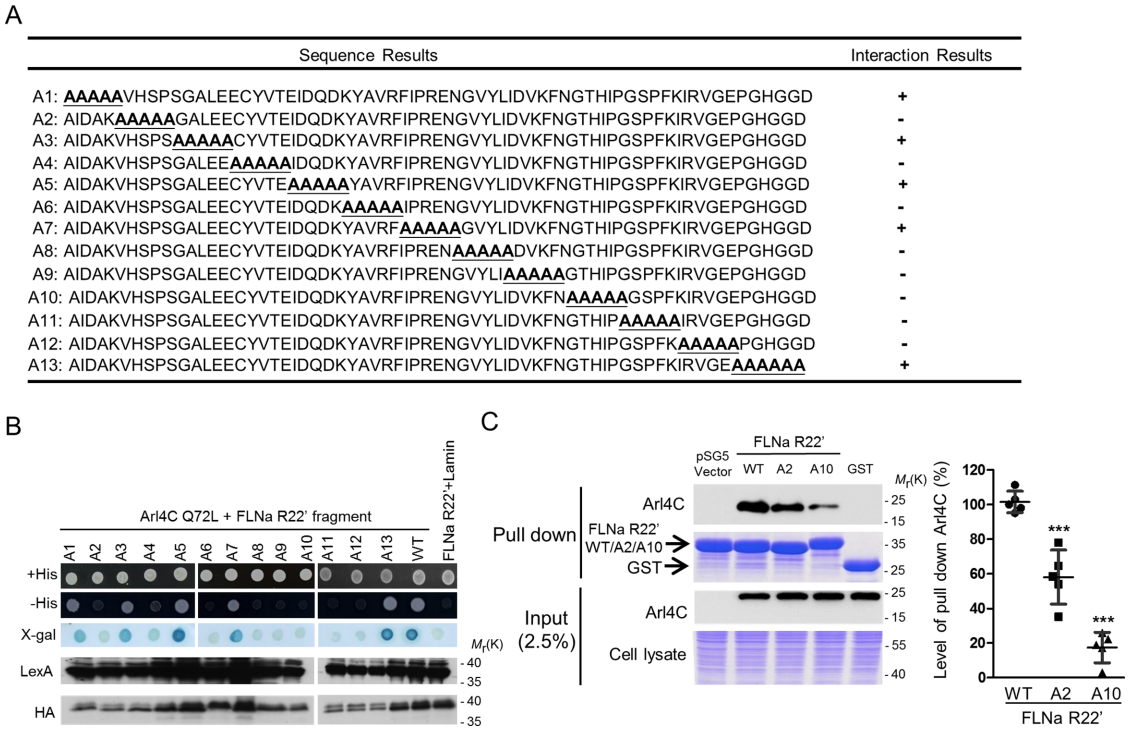

FIGURE 2: Specific IgG repeat 22 (R22) in FLNa is required for interaction with Arl4C. (A) Sequences of FLNa R22 fragments and summary of FLNa R22 interactions with Arl4C-Q72L by alanine scanning. (B) Interactions between Arl4C-Q72L and different FLNa R22 fragments were detected using yeast two-hybrid assays. Interaction between FLNa R22 and Arl4C-Q72L was used as a positive control, and interaction between FLNa R22 and lamin was used as a negative control. Total protein (20 μg) was loaded onto a 10-well gel to detect proteins. (C) Interaction between FLNa R22 mutants and Arl4C-WT was tested by a pull-down assay in HeLa cells. Arl4C immunoblotting results and total cell lysate (input) were used to verify the initial expression level. Equal amounts of GST beads were used in each experiment as verified by Coomassie Blue staining. Quantification of the Arl4C signal in pull-down assays was based on five biological replicates. Scatter plots represent mean ± SD. **, $p < 0.001$ (one-way ANOVA with a post hoc Dunnett's multiple comparison test).

FLNa-knockdown cells, enhanced migration (Figure 6, A and B), indicating that FLNa is critical for Arl4C-induced cell migration.

To ascertain the effect of FLNa-A2 and FLNa-A10 on migration capacity, FLNa in Arl4C-transfected HeLa cells was knocked down by FLNa siRNA, and the ability of FLNa-WT, -A2, and -A10 to rescue the lack of FLNa was examined. The results of wound-healing assays and their quantitative analysis are shown in Figure 6, C and D. The reduction in migration ability due to FLNa knockdown was rescued by overexpressing FLNa-WT, whereas the cells overexpressing FLNa-A2 or FLNa-A10 showed less migration capability. In addition, the migration rescued by FLNa-A10 was much less than that by FLNa-A2 (Figure 6, C and D). The effect of FLNa mutants in cell motility was also performed in A549 cells, which has high expression of endogenous Arl4C, and the results were similar to those in HeLa cells (Figure 6, E and F). Together our data indicated that the Arl4C-FLNa interaction is critical for Arl4C-induced cell migration.

Arl4C-FLNa interaction promotes filopodia formation and cell migration via Cdc42 activation

Among Rho GTPases, the archetypical family member Cdc42 has been known to affect filopodium formation, a process that is closely related to cell motility (Fernandez *et al.*, 2013; Melendez *et al.*, 2013). Thus we tested whether the Arl4C-FLNa interaction promotes Cdc42 or Rac1 activation. A low level of active Cdc42 was detected in cell lysates from HeLa cells. However, Cdc42 activity increased when the cells were transfected with Arl4C, suggesting that expression of Arl4C induces Cdc42 activation (Figure 7A). Active Cdc42 was further increased in cells expressing Arl4C and exogenous myc-FLNa-WT, although the increase in Cdc42 activation due to Arl4C expression was reduced in FLNa-knockdown cells (Figure 7B). These results suggest that FLNa has a role in Arl4C-induced Cdc42 activation.

We next examined the activation of Cdc42 and Rac1 in HeLa cells transfected with Arl4C and FLNa-WT, -A2, or -A10. Cdc42 activity reached a high level after cotransfection of Arl4C and FLNa-WT, whereas the amount of active Cdc42 decreased in cells expressing the FLNa-R22'-A2 and -A10 mutants (Figure 7C). These results indicate that the Arl4C-FLNa interaction plays a critical role in Cdc42 activation. Conversely, the amount of activated Rac1 remained unchanged in HeLa cells overexpressing Arl4C, suggesting that the Arl4C-FLNa interaction does not promote Rac1 activation (Figure 7, A and C). We further used a dominant-negative form of Cdc42, Cdc42 N17, to confirm whether enhanced Cdc42 activity by Arl4C-FLNa interaction is responsible for filopodium formation and cell migration. The expression of Cdc42 N17 reducing the number of filopodia and ability of cell migration was observed in HeLa cells overexpressing Arl4C (Figure 7, D–F). These results indicate that the Arl4C-FLNa interaction affects cell motility through Cdc42 activation.

FGD6 is involved in Arl4C-induced Cdc42 activation

The activation of Cdc42 can be mediated by one of the Cdc42 GEFs, FGD6, which interacts with FLNa and thereby regulates

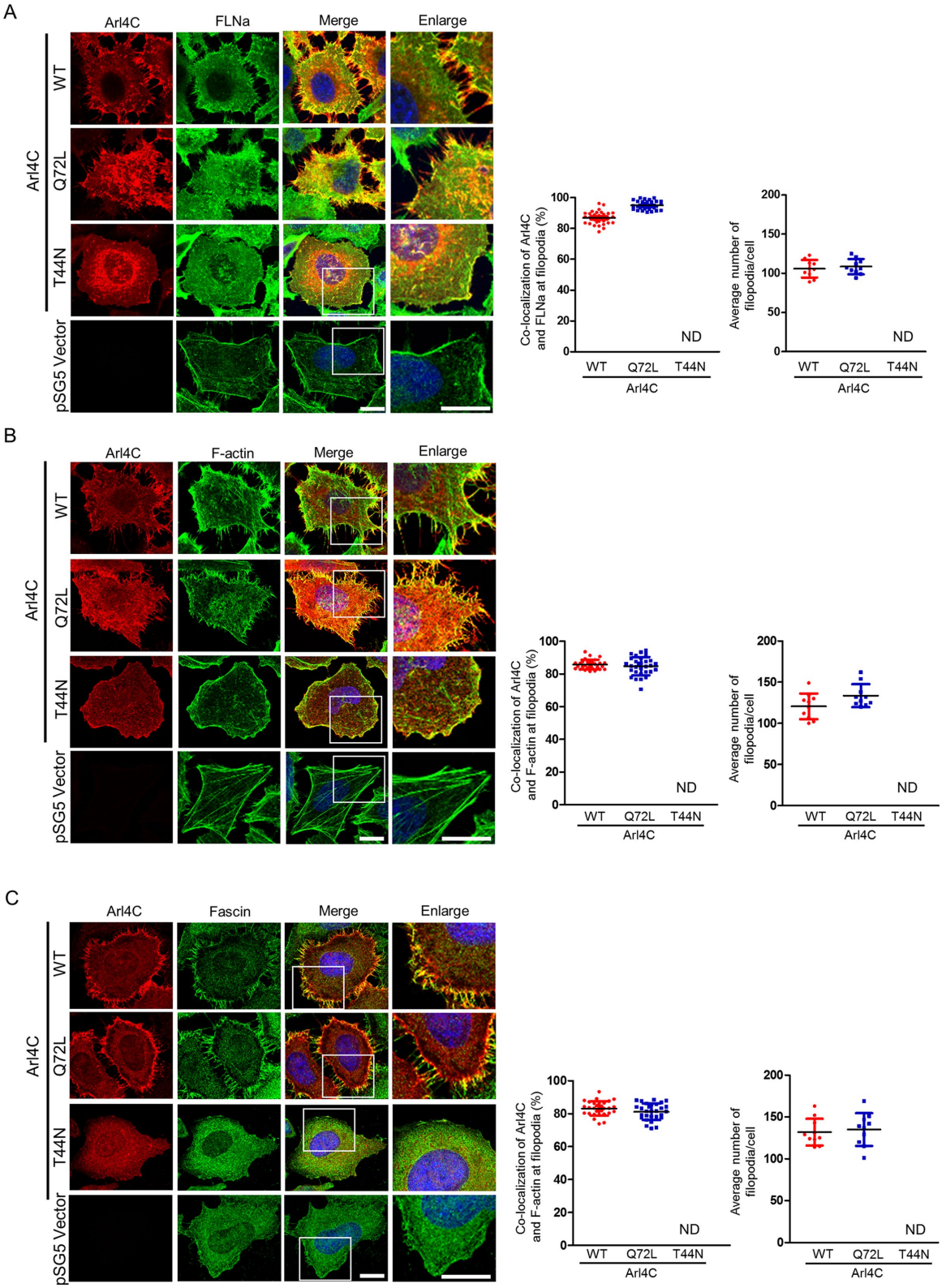

FIGURE 3: Arl4C induces filopodium formation in a nucleotide-dependent manner. Immunofluorescence staining of Arl4C or pSG5 vector in HeLa cells transfected with the indicated plasmids. (A) Cells were stained for Arl4C (red), FLNa (green), and DAPI (blue). (B) Cells were stained for Arl4C (red), phalloidin (green), and DAPI (blue). (C) Cells were stained for Arl4C (red), fascin (green), and DAPI (blue). Scale bar = 10 μm. Histograms: The colocalization ratio of Arl4C and FLNa/F-actin/fascin at filopodia of 10 randomly chosen cells from each group were analyzed in each experiment, and statistical analyses were based on data from three independent experiments (total cells from three experiments = 30). Quantification of the number of filopodia per cell was from three independent experiments (total cells = 10). ND: not detected. Scatter plots represent mean ± SD.

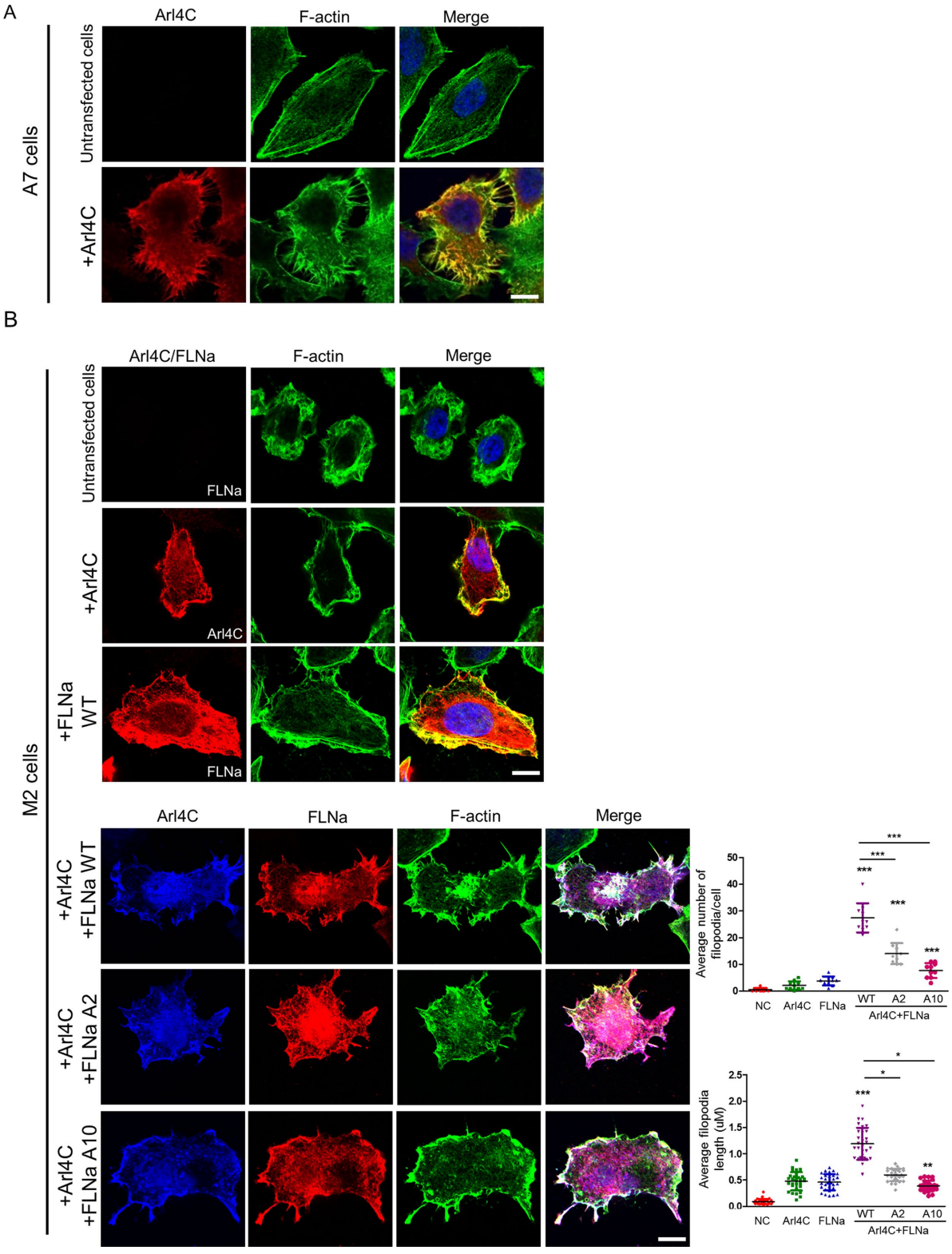

FIGURE 4: Arl4C induces filopodium formation in an FLNa-dependent manner. Representative immunofluorescence images of (A) untransfected and Arl4C-transfected A7 cells and (B) M2 cells untransfected, transfected with Arl4C, full-length FLNa, and cotransfected with full-length FLNa-WT, -A2, and -A10, and Arl4C. Cells were stained for FLNa, Arl4C, phalloidin, and DAPI, respectively. Scale bar = 5 μm. Histograms: The average filopodia length was determined as described in *Materials and Methods*. Ten randomly chosen cells from each group were analyzed in each experiment, and statistical analyses were based on data from three independent experiments (total cells from three experiments = 30). Quantification of number of filopodia per cell was from three independent experiments (total cells = 10). Scatter plots represent mean ± SD. *, $p < 0.05$, **, $p < 0.005$, ***, $p < 0.001$ (one-way ANOVA with a post hoc Dunnett's multiple comparison test).

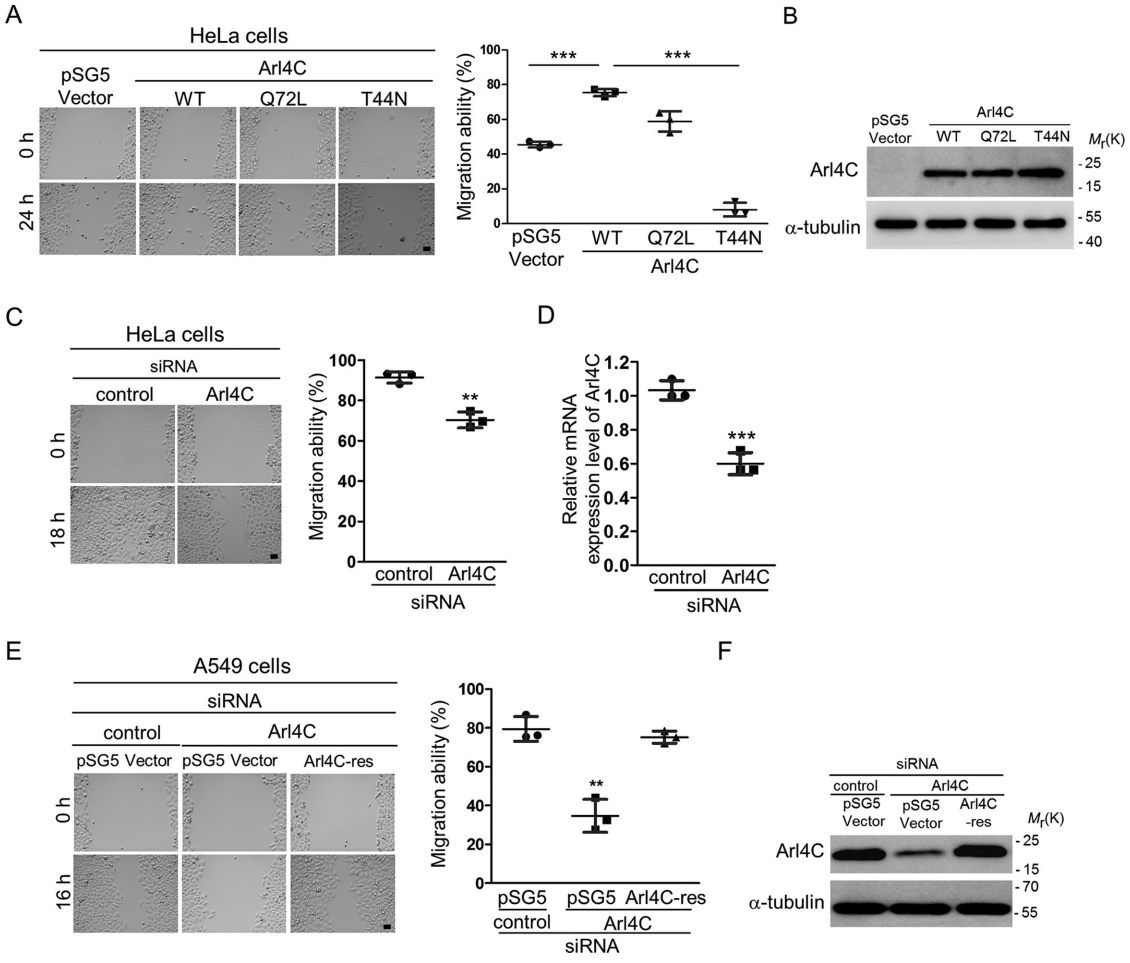

FIGURE 5: Arl4C affects cell migration in a GTP-dependent and GTP/GDP cycling-dependent manner. (A) Representative images of wound-healing assays. HeLa cells transfected with the indicated plasmids for 24 h were subjected to wound-healing migration assays. Migration ability was determined by calculating the change in uncovered area between 0 and 24 h using Metamorph software. Scale bar = 45 μm. (B) Western blot analysis of cell lysates from HeLa cells transfected with the indicated plasmids. Total protein (20 μg) was loaded onto a 10-well gel to detect proteins. (C) Representative images of wound-healing assays. HeLa cells transfected with a control or Arl4C-specific siRNA for 48 h were subjected to wound-healing migration assays. Migration ability was determined by calculating the change in uncovered area between 0 and 18 h using Metamorph software. Scale bar = 45 μm. (D) Q-PCR analysis of mRNA expression of Arl4C in HeLa cells transfected with the indicated siRNAs. GAPDH was used as an internal control. (E) Representative images of wound-healing assays. A549 cells transfected with control siRNA or Arl4C siRNA for 48 h and Arl4C-rescued clone were subjected to wound-healing migration assay. Migration ability was determined by calculating the change in uncovered area between 0 and 16 h using Metamorph software. Scale bar = 45 μm. (F) Western blot analysis of cell lysates from A549 cells transfected with the indicated siRNA or plasmids. Total protein (20 μg) was loaded onto a 10-well gel to detect proteins. The percentages of Arl4C after siRNA treatment are 18.4% ± 0.9%. Histograms in A and E: Quantification of wound-healing migration assays was based on three biological replicates. Scatter plots represent mean ± SD. **, $p < 0.005$, ***, $p < 0.001$ (one-way ANOVA with a post hoc Dunnett's multiple comparison test). Histograms in C and D: Quantification of wound-healing migration assays was based on three biological replicates. Scatter plots represent mean ± SD. **, $p < 0.005$, ***, $p < 0.001$ (two-tailed Student's *t* test).

Cdc42-dependent cell adhesion and podosome formation (Steenblock *et al.*, 2014). Accordingly, we examined whether FGD6 is involved in Arl4C-FLNa interaction-dependent Cdc42 activation. The level of active Cdc42 increased in HeLa cells coexpressing Cdc42 and Arl4C was observed. However, knockdown of FGD6 in cells expressing Arl4C reduced the amount of active Cdc42 (Figure 8A). We further examined whether Arl4C interacting with FLNa affects FGD6-FLNa association to promote Cdc42 activation using immunoprecipitation of FLNa to detect the level of FGD6 in HeLa cells transfected with Arl4C. Compared to cells transfected with pSG5 vector, the level of FGD6 associated with FLNa increased with Arl4C expression (Figure 8B). Although FGD6 was detected in FLNa-knockdown cells rescued by FLNa-WT, less FGD6, as well as Arl4C, was detected in cells rescued by FLNa-A10 (Figure 8C). We further investigated whether similar results could be found in A549 cells. We first observed the level of active Cdc42 decreased in A549 cells depleted of Arl4C. Overexpression of FGD6 in A549 cells, but not in Arl4C-depleted cells, increased the amount of active Cdc42 (Figure 8D). Depletion of Arl4C in A549 cells reduced the FLNa-FGD6 association (Figure 8E). Furthermore, the association of

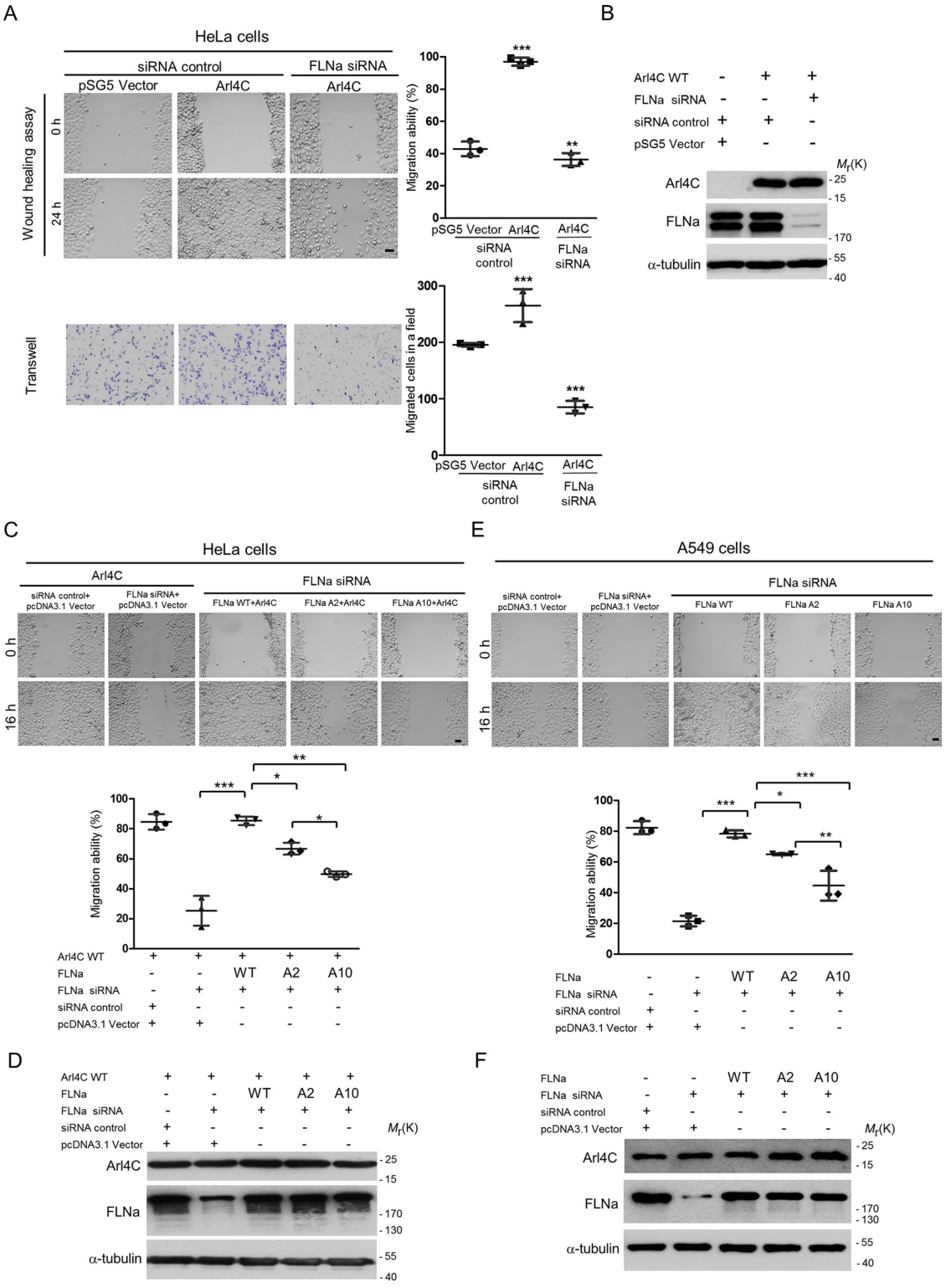

FIGURE 6: Arl4C-FLNa interaction is necessary for cell migration. (A) Representative images of wound-healing and transwell assays of HeLa cells transfected with empty vector, Arl4C, and FLNa siRNA. Confluent monolayers were photographed at the indicated times after wounding. Migration ability was calculated by comparing the area of the wound between 0 and 24 h, as indicated, using Metamorph software. Scale bar = 45 μm. The migrated cells in a field were calculated using ImageJ software after 24 h of migration, as indicated. (B) Immunoblotting analyses were used to verify the level of protein expression in HeLa cells. Total protein (20 μg) was loaded onto a 10-well gel to detect proteins. The percentage of FLNa after siRNA treatment is 23.8 ± 0.67%. (C) Representative images of wound-healing assays of HeLa cells transfected with empty vector, Arl4C, full-length FLNa-WT, -A2, -A10, and FLNa siRNA. Confluent monolayers were photographed at the indicated times after wounding. Migration ability was calculated by comparing the area of the wound between 0 and 16 h, as indicated, using Metamorph

FLNa-FGD6 as well as FLNa-Arl4C was clearly detected in FLNa-knockdown A549 cells rescued by FLNa-WT, but less so in cells rescued by FLNa-A10 (Figure 8F). This result suggests that binding of Arl4C to FLNa may affect the association of FLNa-FGD6. We also showed that no nonspecific binding of Arl4C proteins to IgG and protein G beads was observed in coimmunoprecipitation experiments (Supplemental Figure S1). Taken together, our results suggest that FGD6 is involved in the Arl4C-FLNa interaction-mediated Cdc42 activation.

Next the role of FGD6 in filopodium formation and cell migration was examined. Filopodia were induced in Arl4C-transfected HeLa cells (Figure 9A, top panels), whereas depletion of FGD6 decreased filopodia in cells expressing Arl4C (Figure 9A, bottom panels). Furthermore, depletion of endogenous FGD6 down-regulated cell motility in Arl4C-expressing cells, whereas migration was restored by expression of siRNA-resistant FGD6 (Figure 9, B and C). These results suggest that FGD6 is involved in Arl4C-induced filopodium formation and cell migration.

DISCUSSION

In this study, we identified FLNa as a novel effector of Arl4C and showed that binding between Arl4C and FLNa modulates the formation of filopodia and cell migration. Arl4C expression in FLNa-deficient or FLNa-knockdown cells failed to promote filopodium formation and migration, and the Arl4C-FLNa interaction promoted Cdc42 activation by increasing the association of Cdc42-GEF FGD6 with FLNa. Arl4C expression has been reported to promote tumorigenesis, with its knockdown decreasing the migration ability of human colorectal and lung cancer cell lines (Fujii *et al.*, 2014; Matsumoto *et al.*, 2014). The present study provides an understanding of the mechanism of Alr4C-FLNa function in filopodium formation and cell migration.

FLNa also plays a key role in tumorigenesis as well as the metastatic progression of prostate cancer, ovarian cancer, and gastric carcinoma (Bourguignon *et al.*, 2007; Bedolla *et al.*, 2009; Sun *et al.*, 2014). Deficiency of FLNa in cancer cells significantly decreases their migration and invasion (Jiang *et al.*, 2013); similarly, we also found that migration decreased and filopodia disappeared in Arl4C-transfected HeLa or A7 cells with FLNa knockdown. Conversely, FLNa-deficient M2 cells were able to form filopodia after coexpression of FLNa and Arl4C. Notably, migration regulated by Arl4C and FLNa may involve the same pathway, as overexpression of Arl4C in FLNa-knockdown HeLa cells also down-regulated migration.

FLNa has been reported to interact with more than 70 proteins with broad functional diversity, and this protein may function as an important signaling scaffold by connecting and coordinating a large variety of cellular processes in dynamic regulation of the actin cytoskeleton. Most of its interaction partners associate with FLNa at its C-terminal region (Zhou *et al.*, 2010; Nakamura *et al.*, 2011), and consistent with this, Arl4C also bound to the C-terminal IgG repeat 22 of FLNa. Indeed, mutations in the IgG repeat 22 domain resulted in the loss of the ability to interact with active Arl4C, indicating that those residues are important for the Arl4C-FLNa interaction. However, we cannot rule out the possibility that the mutated residues can cause the destabilization of the structure of R22, rather than the elimination of residues required for the direct interaction with Arl4C. Furthermore, an FLNa mutant deficient in Arl4C binding (FLNa-A10) failed to rescue filopodium formation and cell migration in FLNa-knockdown HeLa cells. These observations support the notion that active Arl4C binding to FLNa IgG repeat 22 modulates the FLNa signaling scaffold to dynamically regulate the actin cytoskeleton.

Matsumoto *et al.* (2014) reported that cell migration promoted by Arl4C expression is regulated by a combination of Wnt/b-catenin and EGF/Ras signaling. Rac1 and Cdc42 are believed to modulate actin polymerization to form peripheral lamellipodia and filopodium protrusions, respectively. Our study demonstrated that the regulation of filopodium formation and migration by the Arl4C-FLNa interaction occurs by promoting the activation of Cdc42, but not Rac1. Although Rac1 had been reported to be involved in modulating cell migration, it plays a slightly different role from Cdc42 in triggering actin-based structural alterations. In fact, Rac1 is mainly required for lamellipodium formation and the induction of membrane ruffles (Nobes and Hall, 1995; Ridley *et al.*, 1999). Moreover, we found that Cdc42 was strongly recruited to the plasma membrane and colocalized with Arl4C in HeLa cells. A similar observation was also reported in another study, whereby Cdc42 was found to accumulate at the leading edge of migrating cells (Osmani *et al.*, 2010).

Several studies have reported that activation of Cdc42 promotes filopodium formation in spinal cord neurons, endothelial cells, and fibroblasts (Brown *et al.*, 2000; Krugmann *et al.*, 2001; Fantin *et al.*, 2015); nonetheless, the molecular mechanism for regulating Cdc42 activity has remained unclear. FGD family members are known to serve as GEFs for Cdc42 activation. In addition to well-known FGD1, FGD6, with high homology to FGD1, is also a Cdc42 GEF. It is reported that FGD6 plays an essential role in osteoclasts by regulating assembly of different actin-based protein networks and activating Cdc42 at different sites. Intracellular signal transduction relies on specific protein–protein interactions to provide accurate protein recruitment and precise subcellular localization; consistent with this notion, our study revealed that the Arl4C-FLNa interaction increased the association of Cdc42-GEF FGD6 with FLNa, which may promote Cdc42 activation. However, different from FGD1, our results demonstrated that FGD6 associated with FLNa may play a role upstream of Cdc42 signaling. Filamin-A has been reported to bind to over 70 proteins, mostly via the same C-terminal region as we report to interact with Arl4C. Whether other FLNa-interacting proteins are affected by the Arl4C-FLNa interaction needs to be further investigated.

software. Scale bar = 45 μm. (D) Immunoblotting analyses were used to verify the level of protein expression in HeLa cells. Total protein (20 μg) was loaded onto a 10-well gel to detect proteins. The percentage of FLNa after siRNA treatment is 37.3 ± 0.6%. (E) Representative images of wound-healing assays of A549 cells transfected with empty vector, full-length FLNa-WT, -A2, -A10, and FLNa siRNA. Confluent monolayers were photographed at the indicated times after wounding. Migration ability was calculated by comparing the area of the wound between 0 and 16 h, as indicated, using Metamorph software. Scale bar = 45 μm. (F) Immunoblotting analyses were used to verify the level of protein expression in A549 cells. Total protein (20 μg) was loaded onto a 10-well gel to detect proteins. The percentage of FLNa after siRNA treatment is 19.7 ± 0.4%. Histograms in A, C, and E: Quantification of migration assays was based on three biological replicates. Scatter plots represent mean ± SD. *, $p < 0.05$, **, $p < 0.005$, ***, $p < 0.001$ (two-tailed Student's *t* test).

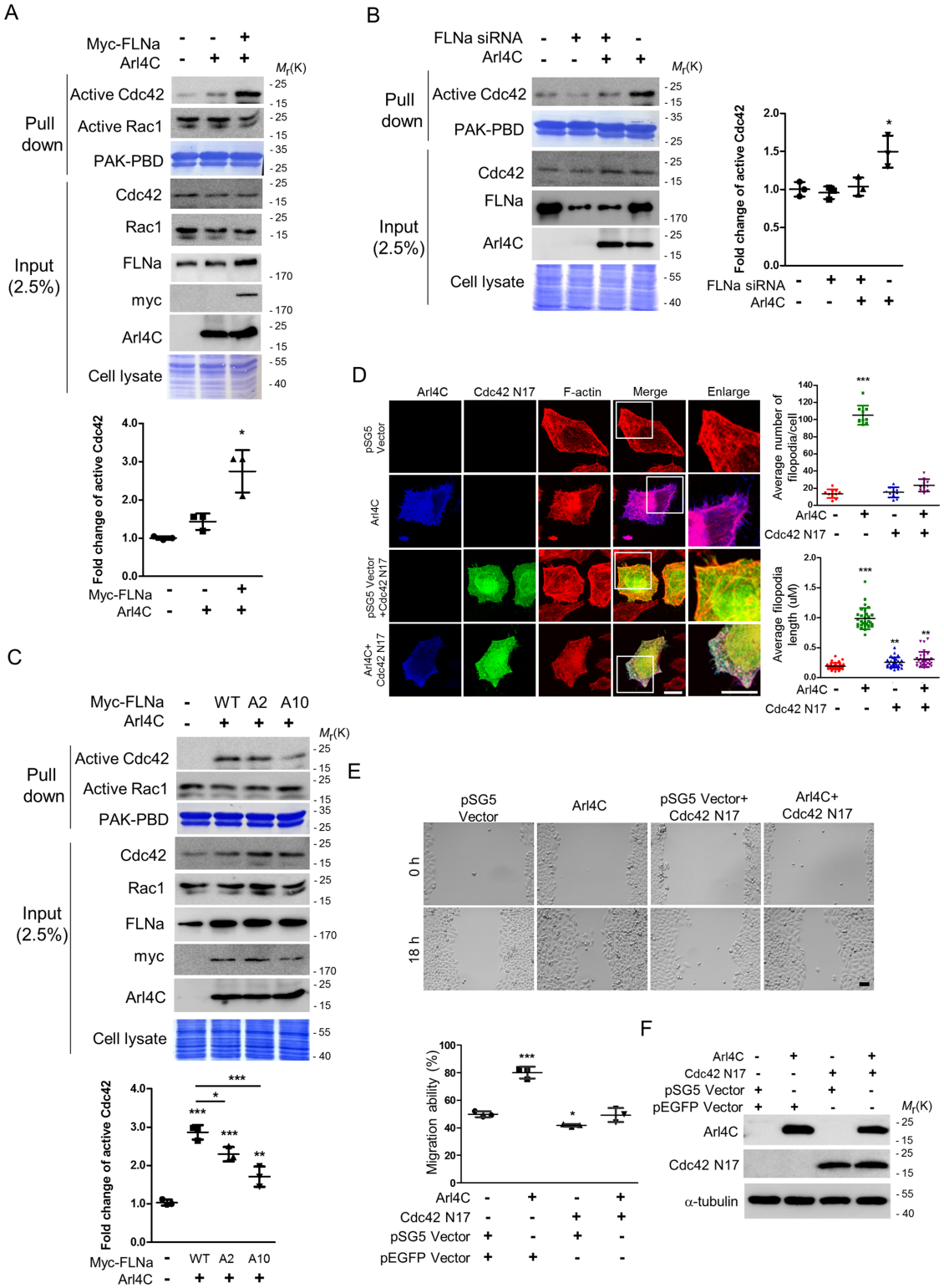

FIGURE 7: Arl4C-FLNa interaction promotes filopodia formation and cell migration through Cdc42 activation. Pull-down assays were performed on HeLa cells transiently transfected with (A) Arl4C-WT and myc-FLNa-WT; (B) Arl4C-WT and FLNa siRNA (the percentage of FLNa after siRNA treatment is 18.4 ± 0.3%); and (C) Arl4C-WT, myc-FLNa-WT, myc-FLNa-A2, and myc-FLNa-A10. Cell lyses followed by pull-down assays were used to examine the cells coexpressing the indicated plasmids. Purified GST fused to PAK1-PBD was incubated with lysates prepared from untransfected and transfected HeLa cells. Interacting proteins bound to the GST beads were analyzed by immunoblotting using the indicated antibodies. SDS–PAGE analysis of total cell lysates and expression of Cdc42, myc-FLNa, and Arl4C (input) by immunoblotting were used to verify the initial expression level. Equal amounts of GST beads were used in each experiment as shown by Coomassie Blue staining. ($n = 3$) Histograms in A–C: Quantification of activity by pull-down assays was based on three biological replicates. Scatter plots

Studies to date have shown that Arl4 subfamily members are involved in vesicle trafficking (Engel *et al.*, 2004; Wei *et al.*, 2009; Lin *et al.*, 2011), organelle structure (Lin *et al.*, 2011; Li *et al.*, 2012), and cytoskeleton organization, similar to the main functions of most Arfs (Donaldson and Jackson, 2011). All Arl4 subfamily members are reported to be actin cytoskeleton regulators (Li *et al.*, 2007; Patel *et al.*, 2011; Matsumoto *et al.*, 2014). Arl4A is implicated in Rac1 signaling via signaling through either cytohesin-2/Arf6 or ELMO/DOCK180, and Arl4D functions upstream of Arf6 through cytohesin-2 GEF in actin organization. These studies demonstrate the cross-talk between Arl4s and the Rho and Arf GTPase pathways.

In conclusion, we demonstrate that Arl4C, but not Arl4A or Arl4D, functions as a novel interacting partner of FLNa to modulate cell motility and the formation of filopodia. The interaction between Arl4C and FLNa occurs in a GTP-dependent manner and regulates filopodium formation and cell migration through Cdc42 (Figure 8D). We conclude that the Arl4C-FLNa interaction promotes Cdc42 activation, which may be through the recruitment of the Cdc42 GEF FGD6. Although we cannot rule out the possibility that Arl4C may be involved in additional signaling pathways, Arl4 proteins appear to act in a specific signaling pathway to orchestrate and fine-tune signal transduction by providing multiple points of integration and to coordinate the action of multiple effectors to control complex cellular processes.

MATERIALS AND METHODS

Antibodies

The preparation of polyclonal antibodies against Arl4A/C/D was described previously (Li *et al.*, 2007). The following primary antibodies were used: anti-FLNa (1:1000, catalogue MAB1678; Millipore, Billerica, MA), anti-alpha tubulin (1:5000, catalogue T5168; Sigma, St. Louis, MO), anti-fascin (1:100, catalogue MAB3582; Millipore), anti-FGD6 (1:200, SC-167891; Santa Cruz Biotechnology, Santa Cruz, CA), anti-Rac1 (1:1000, catalogue 05-389; Millipore), anti-Cdc42 (1:250, catalogue 610929; BD Biosciences, San Jose, CA), anti-myc (1:1000, catalogue MMS-150R; Covance, Princeton, NJ), anti-HA (1:1000, catalogue SC-7392; Santa Cruz Biotechnology), anti-LexA (1:1000, catalogue 5397-1; Clontech, Mountain View, CA), and anti–phalloidin-594 and -488 (1:500, catalogue 8953 and 8878; Cell Signaling). 4′,6-Diamidino-2-phenylindole (DAPI) solution was purchased from Millipore (1:5000, catalogue S7113). Horseradish peroxidase–conjugated goat anti-rabbit and anti-mouse antibodies were purchased from GE Healthcare (1:5000, catalogue NA934V and NA931V; Waukesha, WI). Alexa Fluor 594– and 488–conjugated anti-rabbit or anti-mouse secondary antibodies were purchased from Invitrogen (1:500, catalogue A-11012 for Alexa Fluor 594-rabbit; A-11034 for Alexa Fluor 488-rabbit; A-11001 for Alexa Fluor 488-mouse; A-11032 for Alexa Fluor 594-mouse; Grand Island, NY)

Cell cultures

Human cervical carcinoma HeLa cells were purchased from the American Type Culture Collection (Manassas, VA). Human lung epithelial carcinoma A549 cells were kindly provided by Chia-Jung Yu (Chang Gung University, Taoyuan City, Taiwan). Both HeLa cells and A549 cells were cultured in high-glucose DMEM (HyClone, Logan, UT) supplemented with 10% fetal bovine serum (Li *et al.*, 2007). The FLNa-deficient human melanoma cell line M2 and isogenic FLNa$^+$ cell line A7 (kindly provided by J. Hartwig, Harvard Medical School, Boston, MA) were cultured in α-minimal essential medium supplemented with 8% newborn calf serum and 2% fetal calf serum (HyClone). All cells were maintained at 37°C under an atmosphere containing 5% CO_2. M2 and A7 cells were used at passages 4–10.

Transfection

Cells were transiently transfected with the described plasmids or siRNA using Lipofectamine 2000 transfection reagent (Invitrogen) according to the manufacturer's instructions. All siRNAs were purchased from Dharmacon (GE Healthcare Life Sciences). The specific siRNAs used were as follows: Arl4C: GUGGUGACAUGUUCAGAUU; FGD6: GAAGGGACCGGUUUUAUAA; FLNa: GAAUGGCGUUUACCUGAUU. Cells were harvested at 24 and 48 h after transfection with DNA and siRNA, respectively.

Plasmid construction

cDNAs corresponding to Arl4A/C/D and their various mutants were cloned into the mammalian expression vector pSG5 (Stratagene, La Jolla, CA), which was also used for expressing untagged Arl4C. The cDNAs were also subcloned into the mammalian expression vector pcDNA 3.1 (Invitrogen) or the bacterial expression vector pET15b (Novagen, Madison, WI) and pBTM116 to obtain myc-tagged, His-tagged, or LexA-tagged Arl4 A/C/D and their various mutants. pcDNA 3.1 harboring FLNa-myc was provided by Jeffrey J.Y. Yen (Academia Sinica, Taipei, Taiwan). Partial FLNa DNA fragments were amplified by PCR using syntactic oligonucleotide primers containing restriction enzyme sites. The PCR products were cloned into pACT2, pGEX, and pcDNA 3.0 vectors for transfection. The constructs were confirmed by DNA sequencing.

Total protein extraction and immunoblotting analysis

Total proteins were extracted as described elsewhere (Li *et al.*, 2007). Briefly, transfected cells were harvested, washed, and lysed. After centrifugation, the supernatants were collected and the

represent mean ± SD. *, $p < 0.01$, **, $p < 0.005$. (A) Two-tailed Student's *t* test. (B, C) One-way ANOVA with a post hoc Dunnett's multiple comparison test. (D) Representative images of HeLa cells transfected with indicated plasmids. Cells were stained with Arl4C (blue), Cdc42 N17 (green), and phalloidin (red). Scale bar = 10 μm. Histogram: The average filopodia length was determined as described in *Materials and Methods*. Ten randomly chosen cells from each group were analyzed in each experiment and statistical analyses were based on data from three independent experiments (total cells from three experiments = 30). Quantification of the number of filopodia per cell was from three independent experiments (total cells = 10). Scatter plots represent mean ± SD. ***, $p < 0.001$ (one-way ANOVA with a post hoc Dunnett's multiple comparison test). (E) Representative images of wound-healing assay of HeLa cells transfected with the vector and indicated plasmids. Scale bar = 45 μm. Migration ability was calculated by comparing the area of the wound between 0 and 18 h using Metamorph software. The migrated cells in a field were calculated using ImageJ software after 18 h of migration. Histogram: Quantification of migration assays was based on three biological replicates. Scatter plots represent mean ± SD. *, $p < 0.05$, ***, $p < 0.001$ (one-way ANOVA with a post hoc Dunnett's multiple comparison test). (F) Total protein (20 μg) was loaded onto a 10-well gel to detect proteins. Immunoblotting analyses were used to verify the level of protein expression in HeLa cells transfected with the indicated plasmids.

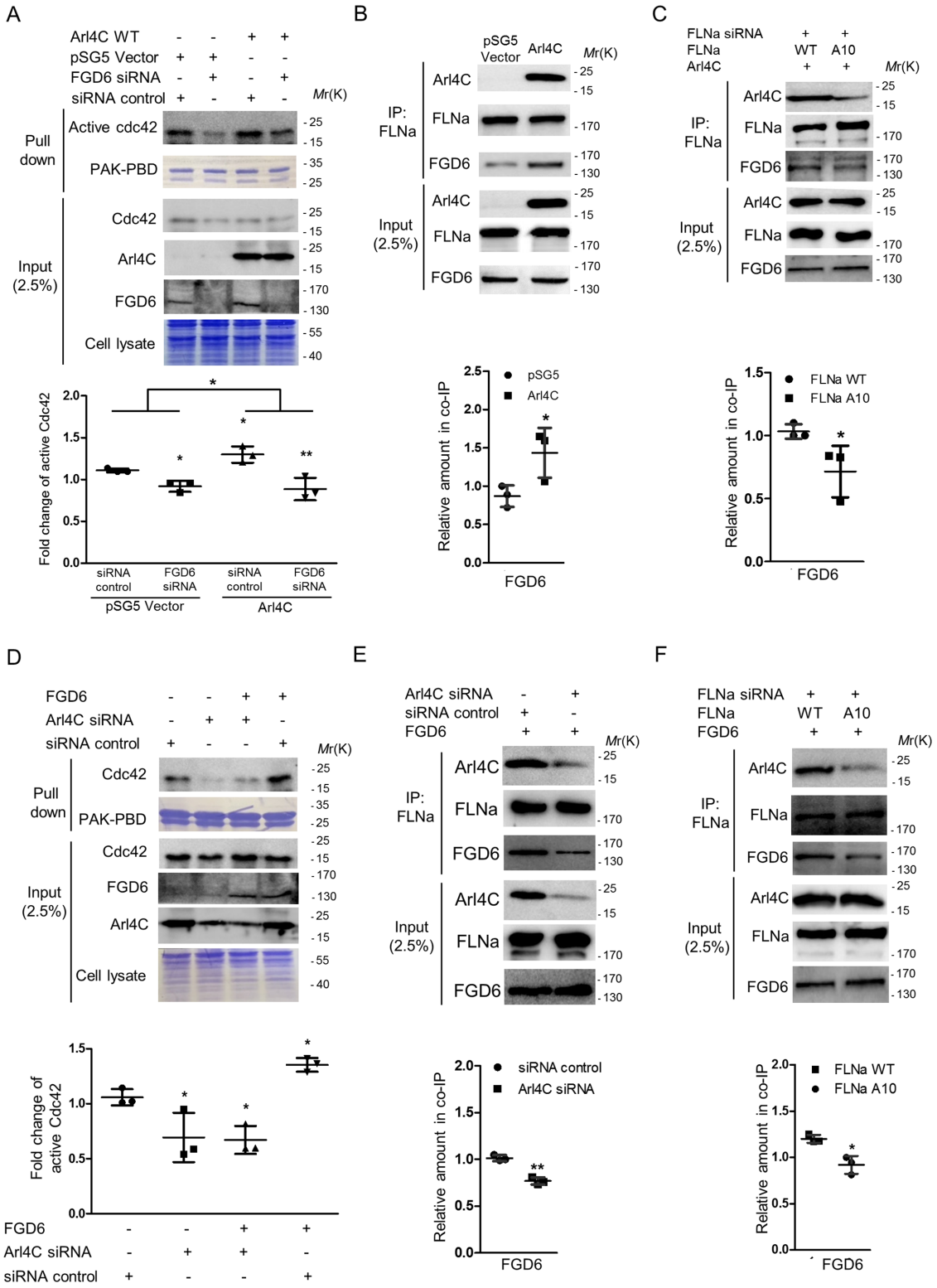

FIGURE 8: Arl4C-FLNa interaction promotes Cdc42 activation via FGD6. (A) Pull-down assays with HeLa cells coexpressing the indicated plasmids or siRNAs were used to detect Cdc42 activation. Total cell lysates and equal amounts of GST beads were analyzed by Coomassie Blue staining. The expression of Cdc42, Arl4C, FGD6 (input), and active Cdc42 was analyzed by immunoblotting. The percentage of FGD6 after siRNA treatment is 14.3 ± 0.7% and 17.4 ± 0.4%. (B) HeLa cells were transiently transfected with the empty vector pSG5 or Arl4C as indicated, interaction was verified by coimmunoprecipitation with anti-FLNa–conjugated protein G magnetic beads. To confirm the initial expression level, 2.5% of the total cell lysate (input) was loaded. SDS–PAGE analysis was used to verify Arl4C, FLNa, and FGD6 expression and bound proteins. (C) HeLa cells were transiently transfected with FLNa siRNA, Arl4C, and full-length FLNa-WT, or -A10; interaction was verified by coimmunoprecipitation with anti-FLNa–conjugated protein G magnetic beads. To confirm the initial expression level, 2.5% of the total cell lysate (input) was loaded. SDS–PAGE

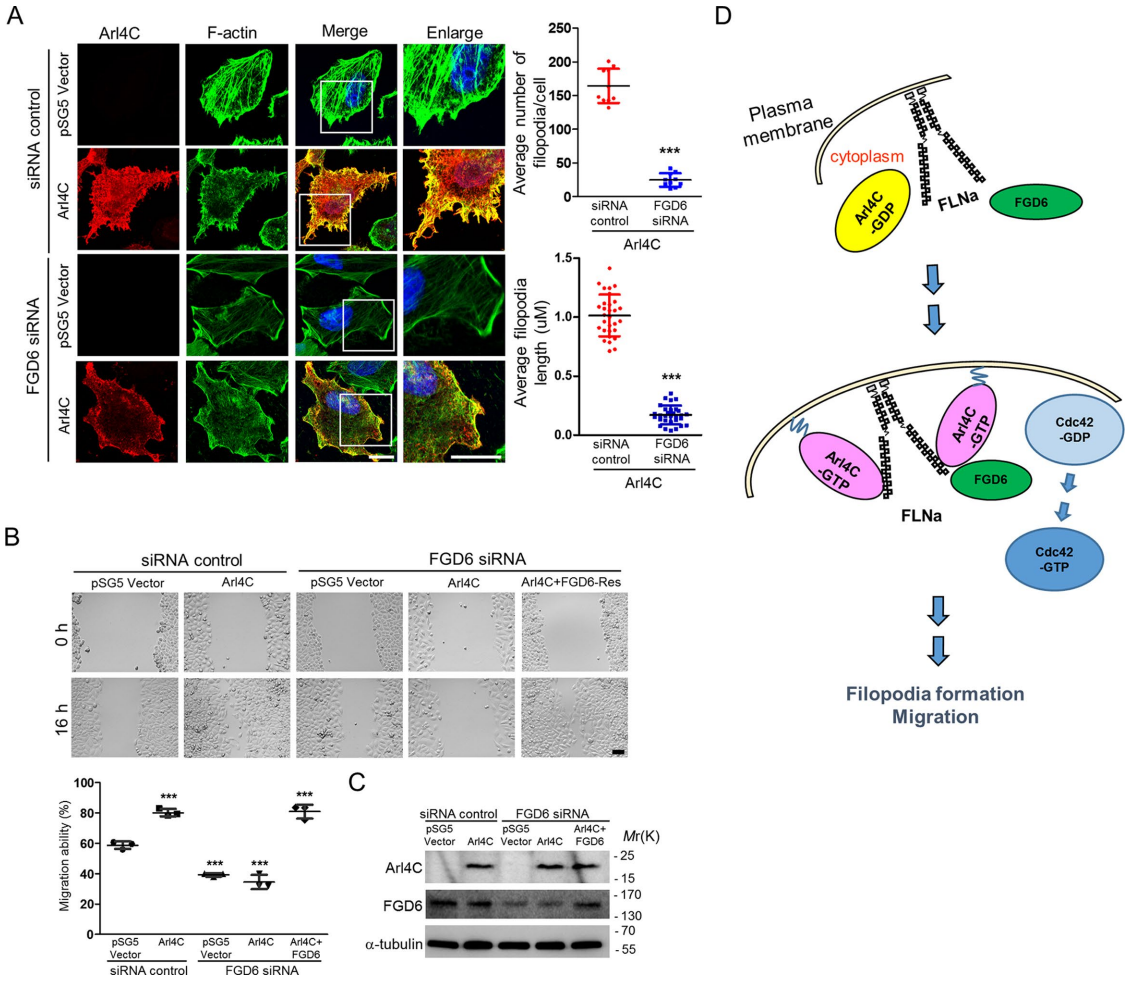

FIGURE 9: Knockdown of FGD6 reduces filopodium formation and cell migration. (A) Representative images of HeLa cells transfected with the indicated plasmids and siRNA. Cells were stained for Arl4C (red), phalloidin (green), and DAPI (blue). Scale bar = 10 μm. Histograms: The average filopodia length was determined as described in *Materials and Methods*. Ten randomly chosen cells from each group were analyzed in each experiment and statistical analyses were based on data from three independent experiments (total cells from three experiments = 30). Quantification of number of filopodia per cell was from three independent experiments (total cells = 10). Scatter plots represent mean ± SD. **, $p < 0.005$ (two-tailed Student's *t* test). (B) Representative images of wound-healing assay. HeLa cells transfected with the indicated plasmids for 16 h were subjected to wound-healing migration assay. Migration ability was determined by calculating the change in uncovered area between 0 and 16 h using Metamorph software. Scale bar = 45 μm. The percentage of FGD6 after siRNA treatment is 26.1 ± 1.4%. Histogram: Quantification of wound-healing migration assays was based on three biological replicates. Scatter plots represent mean ± SD. ***, $p < 0.001$ (one-way ANOVA with a post hoc Dunnett's multiple comparison test). (C) Western blot analysis of cell lysates from HeLa cells transfected with the indicated plasmids or siRNA. Total protein (20 μg) was loaded onto a 10-well gel to detect proteins. (D) A model of Arl4C-FLNa interaction by which FGD6 is recruited to promote Cdc42 activation.

analysis was used to verify Arl4C, FLNa, and FGD6 expression and bound proteins. (D) Pull-down assays with A549 cells coexpressing the indicated plasmids or siRNA were used to detect Cdc42 activation. Total cell lysates and equal amounts of GST beads were analyzed by Coomassie Blue staining. The expression of Cdc42, FGD6, Arl4C (input), and active Cdc42 was analyzed by immunoblotting. The percentage of Arl4C after siRNA treatment is 28.5 ± 0.6% and 29.7 ± 0.8%. (E) A549 cells were transiently transfected with FGD6 or Arl4C siRNA as indicated. The interaction was verified by coimmunoprecipitation with anti-FLNa–conjugated protein G magnetic beads. The percentage of Arl4C after siRNA treatment is 23.6 ± 1.3%. To confirm the initial expression level, 2.5% of the total cell lysate (input) was loaded. SDS–PAGE analysis was used to verify Arl4C, FLNa, and FGD6 expression and bound proteins. (F) A549 cells were transiently transfected with FLNa siRNA, full-length FLNa-WT, or -A10; interaction was verified by coimmunoprecipitation with anti-FLNa–conjugated protein G magnetic beads. To confirm the initial expression level, 2.5% of the total cell lysate (input) was loaded. SDS–PAGE analysis was used to verify Arl4C, FLNa, and FGD6 expression and bound proteins. Histograms in A and D: Quantification of activity by pull-down assays was based on three biological replicates. Scatter plots represent mean ± SD. *, $p < 0.01$, **, $p < 0.005$ (one-way ANOVA with a post hoc Dunnett's multiple comparison test). Histograms in B, C, D, and F: Quantification of co-IP assay or co-IP assay was based on three biological replicates. Scatter plots represent mean ± SD. *, $p < 0.01$, **, $p < 0.005$ (two-tailed Student's *t* test).

protein concentration was determined using a Bio-Rad protein assay kit (Hercules, CA). The proteins in the lysates were separated by 7.5% or 12.5% SDS–PAGE and transferred to Immobilon-P membranes (Millipore). The membranes were blocked for 1 h at room temperature in PBST buffer (0.1% Tween 20 in phosphate-buffered saline [PBS]) containing 5% skim milk powder or bovine serum albumin and then incubated overnight at 4°C in blocking buffer containing appropriately diluted primary antibodies. The membranes were subsequently washed three times in PBST and then incubated in PBST containing an horseradish peroxidase–conjugated secondary antibody (1:5000). After washing, the membranes were developed using enhanced chemiluminescence (Millipore). α-Tubulin was used as an internal control for protein loading.

Total RNA isolation, reverse transcription, and Q-PCR

Total RNAs were extracted using Trizol reagent (Invitrogen). Reverse transcription was performed using a RevertAid H Minus First Strand cDNA Synthesis Kit (Thermo Scientific, Waltham, MA) with a total of 2 μg RNA. The cDNAs were used for quantitative PCR (Q-PCR) with the TaqMan system (Applied Biosystems, Foster City, CA) and Arl4C primer/probe; the housekeeping gene glyceraldehyde-3-phosphate dehydrogenase (GAPDH) was used for normalization.

Yeast two-hybrid screen

A yeast two-hybrid screen was performed as described previously (Fujii *et al.*, 2014). In brief, *Saccharomyces cerevisiae* strain L40 (*MATα trp1 leu2 his3 LYS::(lexAop)4-HIS3 URA3::(lexAop)8-lacZ*) was transformed with LexA-expressing pBTM116 carrying Arl4A/C/D (Lin *et al.*, 2000; Li *et al.*, 2007). A human fetal brain cDNA library in pACT2 (Clontech) was screened using Arl4C-Q72L as the bait. Colonies exhibiting histidine auxotrophy were patched onto selective plates and assayed for β-galactosidase activity using a colony-lift filter assay.

Yeast protein extraction

Yeast cells were harvested after 5 d of culture. Yeast protein extraction was performed as described previously (Su *et al.*, 2015) and the extracted proteins were used for further analysis.

Coimmunoprecipitation

HeLa cells in 10-cm dishes were transiently transfected with 6 μg pSG5-Arl4C WT, 7.2 μg pSG5-Arl4C Q72L, 15 μg pSG5-Arl4C T44N, or 15 μg pSG5 vector using Lipofectamine 2000 transfection reagent. After 16 h of transfection, the cells were lysed with immunoprecipitation (IP) buffer (50 mM Tris-HCl, pH 7.4; 150 mM NaCl; 1% NP-40; 1× protease inhibitor cocktail); the lysate was then centrifuged for 10 min at 14,000 × *g* at 4°C. The supernatants were incubated with protein G magnetic beads (catalogue: LSKMAGG10; Millipore) conjugated with 1 μl of anti-FLNa antibody for 3 h at 4°C using end-over-end agitation and then washed five times with IP buffer. The coimmunoprecipitated proteins were boiled after adding 30 μl 4× protein-loading buffer and analyzed by immunoblotting.

GST pull-down assay

HeLa cells transfected with Arl4A/C/D and their mutants were lysed in pull-down assay buffer containing 50 mM Tris-HCl, pH 7.4, 150 mM NaCl, 1% NP-40, 5 mM dithiothreitol (DTT), and 1× protease inhibitor. An 80-μg sample of GST or GST-FLNa R22′ was incubated with 1 mg cell lysate for at least 2 h at 4°C. The GST beads were then washed five times with assay buffer. The proteins were eluted with protein-loading buffer and analyzed by immunoblotting.

Cdc42/Rac1 activity pull-down assay

Cells transfected with indicated plasmid or siRNA were lysed in activity pull-down assay buffer containing 50 mM Tris-HCl, pH 7.4, 150 mM NaCl, 1% NP-40, 10 mM $MgCl_2$, and 5 mM DTT, and 1× protease inhibitor. A 50-μg sample of GST or GST-PAK-PBD was incubated with 1.75 mg cell lysate for at least 2 h at 4°C. The GST beads were then washed five times with assay buffer. The proteins were eluted with protein-loading buffer and analyzed by immunoblotting.

Immunofluorescence staining

The immunofluorescence staining procedure was performed as previously described (Li *et al.*, 2007). After staining, cells on coverslips were mounted in anti-fade reagent (90% glycerol in PBS containing 1 mg/ml *p*-phenylenediamine). Images were acquired using a Carl Zeiss LSM880 system with with Airyscan (Carl Zeiss MicroImaging, Jena, Germany). For determining colocalization at the filopodia, filopodia were defined as actin-rich finger-like protrusions crossing the cell edge and having fluorescence intensity at least 1.2-fold above background. Confocal images of filopodia were obtained with a Zeiss LSM880 Confocal Upright Microscope with Airyscan with Carl Zeiss objective alpha Plan-Apochromat 100×/1.46 oil DIC VIS-IR and 1.8× optical zoom using Zeiss Zen software according to the manufacturer's instructions. Zen digital imaging software (Zeiss) provides both microscopic image acquisition and processing as well as image data analysis and interpretation as evidenced in other published studies (Merriman *et al.*, 2016; Sullivan *et al.*, 2016; Yap *et al.*, 2016). Only Arl4C/FLNa, Arl4C/F-actin, Arl4C/fascin, or Arl4C/Cdc42-EGFP double-positive cells were imaged for analysis. The procedure for quantitative colocalization of Arl4C/FLNa, Arl4C/F-actin, Arl4C/fascin, or Arl4C/Cdc42-EGFP was done using the Zeiss Microscope Software ZEN 2 (Lu *et al.*, 2012; Marg *et al.*, 2012) and the colocalization coefficients were measured for quantifying colocalization. For each condition, double-positive fluorescence signals at filopodia were selected and reported as regions of interest. For determining each filopodium length, the tips of the filopodia to the internal and protruding parts on the cell body margin were measured. Each filopodium length was measured by using ImageJ software (National Institutes of Health) (Vignjevic *et al.*, 2006). Ten randomly chosen cells from each group were analyzed in each experiment. Ten filopodia in one cell were quantified for average filopodia length per cell. Three biological replicates were quantified for the average filopodia length from 10 cells in each examined group. For colocalization and filopodium length analyses, the number of total cells used for quantification for each condition is presented in the figure legends.

Migration assay

For wound-healing migration assays, cells were seeded in culture medium in six-well plates at a density of (8–10) × 10^5 cells per well. Confluent cells were scratched using a fine pipette tip, washed twice with medium, and observed using a time-lapse microscope (Axiovert 200M; Carl Zeiss MicroImaging) equipped with a temperature and CO_2 controller. The cell migration capacity was determined as described previously (Cunningham *et al.*, 1992) using ImageJ or Metamorph software.

Transwell migration assays were performed as described previously (Steenblock *et al.*, 2014) using the Boyden chamber assay

method, with minor modifications. The lower surface of membranes of the transwell device (8-μm pore size, Corning, Union City, CA) was precoated with fibronectin (50 μg/ml diluted in PBS) at room temperature for at least 45 min. Cells were serum starved for 16 h before seeding into the upper chamber. The migrated cells were stained with 1% crystal violet and counted using a phase-contrast microscope (Eclipse TS-100; Nikon, Melville, NY) equipped with a digital camera (DS-5M, Nikon).

Statistical analysis

All data are presented as the mean ± SD. A one-way analysis of variance (ANOVA) with a post hoc Dunnett's multiple comparison test or two-tailed Student's *t* test was used to analyze differences between each group. All statistical analyses were based on data from independent experiments performed in triplicate. Representative experiments are shown.

ACKNOWLEDGMENTS

This work was supported by grants from the National Science Council, Taiwan (NSC-102 2325-B-002-024), the National Health Research Institutes, Taiwan (NHRI-EX106-10601B1), and Yung-Shin Biomedical Research Funds (YSP-86-019) to F.S.L. We thank J. Hartwig for providing the human melanoma M2 and A7 cell lines, Chia-Jung Yu for providing the human A549 cell line, and Jeffrey J.Y. Yen for providing the FLNa-myc construct in the pcDNA3.1 vector. We also thank Joel Moss, Randy Haun, Chia-Jung Yu, and Ya-Wen Liu for their critical review of the manuscript.

REFERENCES

Bedolla RG, Wang Y, Asuncion A, Chamie K, Siddiqui S, Mudryj MM, Prihoda TJ, Siddiqui J, Chinnaiyan AM, Mehra R, *et al.* (2009). Nuclear versus cytoplasmic localization of filamin A in prostate cancer: immunohistochemical correlation with metastases. Clin Cancer Res 15, 788–796.

Bourguignon LY, Gilad E, Peyrollier K (2007). Heregulin-mediated ErbB2-ERK signaling activates hyaluronan synthases leading to CD44-dependent ovarian tumor cell growth and migration. J Biol Chem 282, 19426–19441.

Brown MD, Cornejo BJ, Kuhn TB, Bamburg JR (2000). Cdc42 stimulates neurite outgrowth and formation of growth cone filopodia and lamellipodia. J Neurobiol 43, 352–364.

Burd CG, Strochlic TI, Gangi Setty SR (2004). Arf-like GTPases: not so Arf-like after all. Trends Cell Biol 14, 687–694.

Cunningham CC, Gorlin JB, Kwiatkowski DJ, Hartwig JH, Janmey PA, Byers HR, Stossel TP (1992). Actin-binding protein requirement for cortical stability and efficient locomotion. Science 255, 325–327.

Donaldson JG, Jackson CL (2000). Regulators and effectors of the ARF GTPases. Curr Opin Cell Biol 12, 475–482.

Donaldson JG, Jackson CL (2011). ARF family G proteins and their regulators: roles in membrane transport, development and disease. Nat Rev Mol Cell Biol 12, 362–375.

D'Souza-Schorey C, Chavrier P (2006). ARF proteins: roles in membrane traffic and beyond. Nat Rev Mol Cell Biol 7, 347–358.

Engel T, Luekena A, Bode G, Hobohmc U, Lorkowskia S, Schlueterb B, Rusta S, Cullena P, Pechc M, Assmanna G, *et al.* (2004). ADP-ribosylation factor (ARF)-like 7 (ARL7) is induced by cholesterol loading and participates in apolipoprotein AI-dependent cholesterol export. FEBS Lett 566, 241–246.

Fantin A, Lampropoulou A, Gestri G, Raimondi C, Senatore V, Zachary I, Ruhrberg C (2015). NRP1 regulates CDC42 activation to promote filopodia formation in endothelial tip cells. Cell Rep 11, 1577–1590.

Fernandez D, Horrillo A, Alquezar C, Gonzalez-Manchon C, Parrilla R, Ayuso MS (2013). Control of cell adhesion and migration by podocalyxin. Implication of Rac1 and Cdc42. Biochem Biophys Res Commun 432, 302–307.

Friedl P, Wolf K (2003). Tumour-cell invasion and migration: diversity and escape mechanisms. Nat Rev Cancer 3, 362–374.

Fujii S, Matsumoto S, Nojima S, Morii E, Kikuchi A (2014). Arl4c expression in colorectal and lung cancers promotes tumorigenesis and may represent a novel therapeutic target. Oncogene 34, 4834–4844.

Gehler S, Baldassarre M, Lad Y, Leight JL, Wozniak MA, Riching KM, Eliceiri KW, Weaver VM, Calderwood DA, Keely PJ (2009). Filamin A–β1 integrin complex tunes epithelial cell response to matrix tension. Mol Biol Cell 20, 3224–3238.

Heasman SJ, Ridley AJ (2008). Mammalian Rho GTPases: new insights into their functions from *in vivo* studies. Nat Rev Mol Cell Biol 9, 690–701.

Himmel M, Van Der Ven PF, Stocklein W, Furst DO (2003). The limits of promiscuity: isoform-specific dimerization of filamins. Biochemistry 42, 430–439.

Jackson CL, Casanova JE (2000). Turning on ARF: the Sec7 family of guanine-nucleotide-exchange factors. Trends Cell Biol 10, 60–67.

Jacobs S, Schilf C, Fliegert F, Koling S, Weber Y, Schurmann A, Joost HG (1999). ADP-ribosylation factor (ARF)-like 4, 6, and 7 represent a subgroup of the ARF family characterization by rapid nucleotide exchange and a nuclear localization signal. FEBS Lett 456, 384–388.

Jiang X, Yue J, Lu H, Campbell N, Yang Q, Lan S, Haffty BG, Yuan C, Shen Z (2013). Inhibition of filamin-A reduces cancer metastatic potential. Int J Biol Sci 9, 67–77.

Kahn RA, Cherfils J, Elias M, Lovering RC, Munro S, Schurmann A (2006). Nomenclature for the human Arf family of GTP-binding proteins: ARF, ARL, and SAR proteins. J Cell Biol 172, 645–650.

Krugmann S, Jordens I, Gevaert K, Driessens M, Vandekerckhove J, Hall A (2001). Cdc42 induces filopodia by promoting the formation of an IRSp53:Mena complex. Curr Biol 11, 1645–1655.

Lauffenburger DA, Horwitz AF (1996). Cell migration: a physically integrated molecular process. Cell 84, 359–369.

Li CC, Chiang TC, Wu TS, Pacheco-Rodriguez G, Moss J, Lee FJ (2007). ARL4D recruits cytohesin-2/ARNO to modulate actin remodeling. Mol Biol Cell 18, 4420–4437.

Li CC, Wu TS, Huang CF, Jang LT, Liu YT, You ST, Liou GG, Lee FJ (2012). GTP-binding-defective ARL4D alters mitochondrial morphology and membrane potential. PLoS One 7, e43552.

Lin CY, Huang PH, Liao WL, Cheng HJ, Huang CF, Kuo JC, Pattoni WT, Massenburgi D, Mossi J, Lee FJ (2000). ARL4, an ARF-like protein that is developmentally regulated and localized to nuclei and nucleoli. J Biol Chem 275, 37815–37823.

Lin YC, Chiang TC, Liu YT, Tsai YT, Jang LT, Lee FJ (2011). ARL4A acts with GCC185 to modulate Golgi complex organization. J Cell Sci 124, 4014–4026.

Lin CY, Li CC, Huang PH, Lee FJ (2002). A developmentally regulated ARF-like 5 protein (ARL5), localized to nuclei and nucleoli, interacts with heterochromatin protein 1. J Cell Sci 115, 4433–4445.

Lu D, Sun HQ, Wang H, Barylko B, Fukata Y, Fukata M, Albanesi JP, Yin HL (2012). Phosphatidylinositol 4-kinase IIα is palmitoylated by Golgi-localized palmitoyltransferases in cholesterol-dependent manner. J Biol Chem 287, 21856–21865.

Lynch CD, Gauthier NC, Biais N, Lazar AM, Roca-Cusachs P, Yu CH, Sheetz MP (2011). Filamin depletion blocks endoplasmic spreading and destabilizes force-bearing adhesions. Mol Biol Cell 22, 1263–1273.

Marg A, Schoewel V, Timmel T, Schulze A, Shah C, Daumke O, Spuler S (2012). Sarcolemmal repair is a slow process and includes EHD2. Traffic 13, 1286–1294.

Matsumoto S, Fujii S, Sato A, Ibuka S, Kagawa Y, Ishii M, Kikuchi A (2014). A combination of Wnt and growth factor signaling induces Arl4c expression to form epithelial tubular structures. EMBO J 33, 702–718.

Melendez J, Liu M, Sampson L, Akunuru S, Han X, Vallance J, Witte D, Shroyer N, Zheng Y (2013). Cdc42 coordinates proliferation, polarity, migration, and differentiation of small intestinal epithelial cells in mice. Gastroenterology 145, 808–819.

Merriman C, Huang Q, Rutter GA, Fu D (2016). Lipid-tuned Zinc transport activity of human ZnT8 protein correlates with risk for Type-2 diabetes. J Biol Chem 291, 26950–26957.

Moss J, Vaughan M (1998). Molecules in the ARF orbit. J Biol Chem 273, 21431–21434.

Nakamura F, Stossel TP, Hartwig JH (2011). The filamins: organizers of cell structure and function. Cell Adh Migr 5, 160–169.

Nobes CD, Hall A (1995). Rho, rac, and cdc42 GTPases regulate the assembly of multimolecular focal complexes associated with actin stress fibers, lamellipodia, and filopodia. Cell 81, 53–62.

Osmani N, Peglion F, Chavrier P, Etienne-Manneville S (2010). Cdc42 localization and cell polarity depend on membrane traffic. J Cell Biol 191, 1261–1269.
Pasqualato S, Renault L, Cherfils J (2002). Arf, Arl, Arp and Sar proteins: a family of GTP-binding proteins with a structural device for "front–back" communication. EMBO Rep 3, 1035–1041.
Patel M, Chiang TC, Tran V, Lee FJ, Cote JF (2011). The Arf family GTPase Arl4A complexes with ELMO proteins to promote actin cytoskeleton remodeling and reveals a versatile Ras-binding domain in the ELMO proteins family. J Biol Chem 286, 38969–38979.
Ridley AJ, Allen WE, Peppelenbosch M, Jones GE (1999). Rho family proteins and cell migration. Biochem Soc Symp 65, 111–123.
Schurmann A, Breiner M, Becker W, Huppertz C, Kainulainen H, Kentrup H, Joost HG (1994). Cloning of two novel ADP-ribosylation factor-like proteins and characterization of their differential expression in 3T3-L1 cells. J Biol Chem 269, 15683–15688.
Seo MD, Seok SH, Im H, Kwon AR, Lee SJ, Kim HR, Cho Y, Park D, Lee BJ (2009). Crystal structure of the dimerization domain of human filamin A. Proteins 75, 258–263.
Steenblock C, Heckel T, Czupalla C, Espirito Santo AI, Niehage C, Sztacho M, Hoflack B (2014). The Cdc42 guanine nucleotide exchange factor FGD6 coordinates cell polarity and endosomal membrane recycling in osteoclasts. J Biol Chem 289, 18347–18359.
Stossel TP, Condeelis J, Cooley L, Hartwig JH, Noegel A, Schleicher M, Shapiro SS (2001). Filamins as integrators of cell mechanics and signalling. Nat Rev Mol Cell Biol 2, 138–145.
Su D, Katsaros D, Xu S, Xu H, Gao Y, Biglia N, Feng J, Ying L, Zhang P, Benedetto C, *et al*. (2015). ADP-ribosylation factor-like 4C (ARL4C), a novel ovarian cancer metastasis suppressor, identified by integrated genomics. Am J Transl Res 7, 242–256.
Sullivan CS, Kumper M, Temple BS, Maness PF (2016). The Neural Cell Adhesion Molecule (NCAM) promotes clustering and activation of EphA3 receptors in GABAergic interneurons to induce Ras homolog gene family, member a (RhoA)/Rho-associated protein kinase (ROCK)-mediated growth cone collapse. J Biol Chem 291, 26262–26272.
Sun GG, Sheng SH, Jing SW, Hu WN (2014). An antiproliferative gene FLNA regulates migration and invasion of gastric carcinoma cell in vitro and its clinical significance. Tumour Biol 35, 2641–2648.
Takai Y, Sasaki T, Matozaki T (2001). Small GTP-binding proteins. Physiol Rev 81, 153–208.
Van Der Flier A, Sonnenberg A (2001). Structural and functional aspects of filamins. Biochim Biophys Acta 1538, 99–117.
Vignjevic D, Kojima S, Aratyn Y, Danciu O, Svitkina T, Borisy GG (2006). Role of fascin in filopodial protrusion. J Cell Biol 174, 863–875.
Wei SM, Xie CG, Abe Y, Cai JT (2009). ADP-ribosylation factor like 7 (ARL7) interacts with alpha-tubulin and modulates intracellular vesicular transport. Biochem Biophys Res Commun 384, 352–356.
Yap CC, Digilio L, Mcmahon L, Roszkowska M, Bott CJ, Kruczek K, Winckler B (2016). Different doublecortin (DCX) patient alleles show distinct phenotypes in cultured neurons: evidence for divergent loss-of-function and "off-pathway" cellular mechanisms. J Biol Chem 291, 26613–26626.
Zhou AX, Hartwig JH, Akyurek LM (2010). Filamins in cell signaling, transcription and organ development. Trends Cell Biol 20, 113–123.